

# Characterization of the electronic ground state of $\text{Mg}_2^+$ by PFI-ZEKE photoelectron spectroscopy

Matthieu Génévriez,<sup>1,2</sup> Maxime Holdener,<sup>2</sup> Carla Kreis,<sup>2</sup> and Frédéric Merkt<sup>2</sup>

<sup>1</sup>*Institute of Condensed Matter and Nanosciences,*

*Université catholique de Louvain, Louvain-la-Neuve B-1348, Belgium*

<sup>2</sup>*Laboratory of Physical Chemistry, ETH Zurich, CH-8093 Zurich, Switzerland*

The  $X^+ \ ^2\Sigma_u^+$  ground electronic state of the  $\text{Mg}_2^+$  ion has been studied by pulsed-field-ionization zero-kinetic-energy (PFI-ZEKE) photoelectron spectroscopy. Rotationally cold  $\text{Mg}_2$  molecules produced in a laser-ablation supersonic-expansion source were ionized by resonant two-photon absorption from the  $X \ ^1\Sigma_g^+(v''=0)$  ground vibronic state. The photoelectron spectra of the  $v^+ = 3 - 14$  vibrational levels of the  $X^+$  state were recorded with rotational resolution and their analysis led to the determination of accurate term values and rotational constants for these levels. Improved values of the adiabatic ionization energy of  $^{24}\text{Mg}_2$  ( $51\,503.9(4) \text{ cm}^{-1}$ ) and of the ground-state dissociation energy of  $^{24}\text{Mg}_2^+$  ( $10\,572.3(6) \text{ cm}^{-1}$ ) were determined from experimental data.

## I. INTRODUCTION

Alkaline-earth-metal diatomic molecules have been extensively studied (see, *e.g.*, [1–5]). They have a very weakly bound ground electronic state and unusual chemical properties [3]. For example, simple molecular-orbital theory fails to describe the chemical bond of the ground state of  $\text{Be}_2$  [6, 7] and the calculation of the potential-energy functions of this few-electron molecule to the level of accuracy reached experimentally is still a challenge for *ab initio* quantum chemical methods [3, 8]. The alkaline-earth-metal atoms ( $M=\text{Be, Mg, Ca, Sr, Ba}$ ) and their singly charged ions  $M^+$  can easily be laser cooled [9–13] and the accurate knowledge of the properties of the alkaline-earth-metal dimers ( $M_2$ ) and their ions ( $M_2^+$ ) is important for characterizing atomic collisions in ultracold gases. For example, scattering lengths are related to the properties of the molecular potential-energy functions at large internuclear distances (see Ref. 14 for an example with  $\text{Mg}_2$ ). The accurate knowledge of molecular structure is also required when designing photoassociation schemes used to produce molecules in ultracold atomic ensembles [15–17]. For these reasons, the ground and first-excited states of  $\text{Mg}_2$  have been thoroughly characterized by high-resolution spectroscopy, and highly accurate potential-energy functions were derived from experimental data [2, 18], building upon earlier measurements of the absorption and laser-induced-fluorescence spectra of  $\text{Mg}_2$  [19–22].

In contrast to the neutral species, little is known on the singly charged alkaline-earth-metal diatomic cations  $M_2^+$ . The ground electronic state of  $\text{Be}_2^+$  was investigated by pulsed-field-ionization zero-kinetic-energy photoelectron spectroscopy (PFI-ZEKE-PES) [23] and the ground-state potential-well depth ( $D_e$ ) of  $\text{Sr}_2^+$  was determined from the photoionization spectra of  $\text{Sr}_2$  [24]. Experimental investigations of  $\text{Mg}_2^+$  are limited to a photodissociation study, which led to the determination of the ground-state dissociation energy ( $D_0 = 10\,200 \pm 300 \text{ cm}^{-1}$ ) [25]. Most of what is known on this ion was obtained in high-level *ab initio* calculations [5, 26–31]. The development of hybrid

ion-atom traps, accommodating both ultracold atomic gases and trapped ions (see, *e.g.*, [32–34]) has prompted the need of further studies of alkaline-earth-metal dimer ions because, as for the neutral molecule case, molecular potential-energy functions play an important role in the description of cold collisions and photoassociation within the trap [35].

The knowledge of the ground electronic state of  $\text{Mg}_2^+$  is also required as a starting point to study the electronically excited states of the ion, and in particular the Rydberg series converging to the metastable levels of the  $\text{Mg}_2^{2+}$  ion [36], which have not been observed so far. We plan to study these states following the procedure we used recently to characterize the ground electronic state of  $\text{MgAr}^{2+}$  and the Rydberg series of  $\text{MgAr}^+$  converging to this doubly charged ion [37–42].

We report an experimental study of the  $X^+ \ ^2\Sigma_u^+$  ground electronic state of  $\text{Mg}_2^+$  by high-resolution PFI-ZEKE-PES [43–46]. Ground-state  $\text{Mg}_2$  molecules formed in a laser-ablation supersonic-expansion source were excited to the region of the  $\text{Mg}_2^+(X^+)$  ionization threshold by resonant two-photon excitation, as described in detail in Sec. II. Rotationally resolved photoelectron spectra were recorded for the  $v^+ = 3 - 14$  vibrational levels of the ion. They are presented and analyzed in Sec. III. Molecular constants including the dissociation energy of  $\text{Mg}_2^+(X^+)$ , its vibrational and rotational constants and the adiabatic ionization potential of  $\text{Mg}_2$  are derived and compared to available data. Our results provide a comprehensive and accurate description for the ground-electronic state of  $\text{Mg}_2^+$ .

## II. EXPERIMENT

The experimental setup used in the present work is based on the one used to study  $\text{Mg}$  and  $\text{MgAr}$  ions, as described in Refs. 47, 48, and was adapted to the production of  $\text{Mg}_2$  molecules and ions.  $\text{Mg}_2$  dimers are formed by laser ablation of a  $\text{Mg}$  rod within the nozzle of a supersonic-expansion source with  $\text{Ne}$  used as carrier gas.

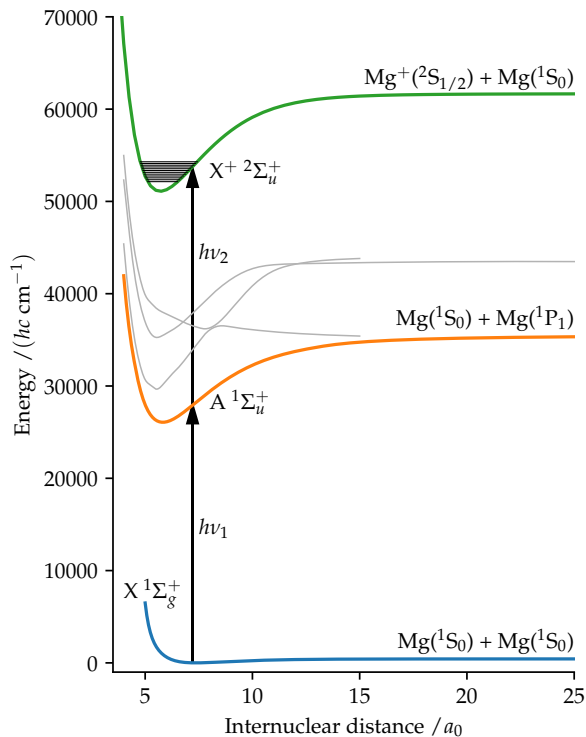


FIG. 1. Potential-energy functions of the electronic states of  $\text{Mg}_2$  and of the ground electronic state of  $\text{Mg}_2^+$  relevant for the present investigation. The functions of the X and A states of  $\text{Mg}_2$  were calculated using the model potentials and parameters from Refs. 2 and 18, respectively. The gray potential-energy curves correspond to higher-lying singlet ungerade states of  $\text{Mg}_2$  calculated in Ref. 50. The potential-energy function of the  $X^+$  state of  $\text{Mg}_2^+$  is from Ref. 30. The two-photon ionization scheme used in the experiment is illustrated by the vertical arrows. The full horizontal lines in the  $X^+$ -state potential-energy function represent the vibrational levels measured in the present work.

Ablation is carried out by focusing the second harmonic of a nanosecond pulsed Nd:YAG laser (repetition rate 25 Hz) onto the Mg rod with an  $f = 30$  cm lens. A pulse energy of  $\sim 10$  mJ was found to be an optimal compromise to simultaneously reach a large  $\text{Mg}_2$  number density, low shot-to-shot fluctuations and a long-term stability of the ablation process. As is common for metal-cluster laser-ablation sources [49], the nozzle was chosen to be a narrow (1-mm diameter) and long (15-mm) tube along the molecular-beam-propagation direction such that the metal-vapor density remained large over a significant distance to increase metal-dimer formation. We observed that this growth channel significantly reduces the shot-to-shot fluctuations of the  $\text{Mg}_2$  density in the molecular beam. 6.5 cm beyond the nozzle orifice, the molecular beam is collimated by a 3-mm-diameter skimmer before it enters the photoexcitation chamber.

In this chamber, the molecular beam is intersected at right angles by two tuneable dye lasers pumped by the

second harmonic of a seeded Q-switched Nd:YAG laser. The photoexcitation scheme depicted in Fig. 1 is used to excite the  $\text{Mg}_2$  molecules from their  $X^+ 1\Sigma_g^+$  ground state to the region of the first ionization thresholds using two tuneable lasers in a resonant  $(1 + 1')$  two-photon absorption process. The first dye laser, called Laser 1 hereafter, is operated with Pyridine 1 and 2 dyes and its fundamental output is frequency-doubled in a beta-barium-borate (BBO) crystal to generate radiation with wavenumber tuneable in the range from  $\tilde{\nu}_1 = 27000$   $\text{cm}^{-1}$  to  $28000$   $\text{cm}^{-1}$ . The frequency-doubled output is used to excite  $\text{Mg}_2$  molecules in their electronic ground state ( $X^+ 1\Sigma_g^+$ ) to the first electronically excited state ( $A^+ 1\Sigma_u^+$ ). The second laser, called Laser 2, is operated with Styryl 11 dye and its output is also frequency doubled in a BBO crystal to generate radiation in the range from  $\tilde{\nu}_2 = 24500$   $\text{cm}^{-1}$  to  $26500$   $\text{cm}^{-1}$ . This radiation is used to further excite the  $\text{Mg}_2$  molecules from the  $A^+ 1\Sigma_u^+$  state to high Rydberg states located energetically just below rovibrational levels of the  $X^+ 2\Sigma_u^+$  ground electronic state of the  $\text{Mg}_2^+$  molecular ion. The wavenumbers of the fundamental outputs of both dye lasers were calibrated using a commercial wavemeter with a specified absolute accuracy of  $0.02$   $\text{cm}^{-1}$ . The pulse energy of the frequency-doubled output of Laser 1 was kept below  $\sim 50$   $\mu\text{J}$  to avoid power broadening of the  $A \leftarrow X$  transition and ionization of molecules in the A state by absorption of a further photon of the same wavenumber.

Photoexcitation occurs within a stack of 5 cylindrical resistively coupled electrodes surrounded by two concentric mu-metal shields to suppress stray magnetic fields. Electric potentials applied to the stack generate electric fields in the interaction region that serve either to field-ionize molecules in high Rydberg states and accelerate the electrons into a flight tube or to extract the  $\text{Mg}_2^+$  ions produced by photoionization, depending on the sign of the potential difference. Charged particles are detected at the end of the flight tube by a microchannel-plate detector. The different masses, and in particular those associated with the various  $\text{Mg}_2^+$  isotopomers ( $^{24,25,26}\text{Mg}$ ), are separated by their times of flight. Natural abundances  $N_{m_1, m_2}$  of the  $^{m_1}\text{Mg}^{m_2}\text{Mg}$  isotopomers can be calculated from those of the Mg isotopes ( $N_{24} = 0.7899(4)$ ,  $N_{25} = 0.1000(1)$ , and  $N_{26} = 0.1101(3)$  [51]), which gives  $N_{24,24} = 0.624$ ,  $N_{24,25} = 0.158$ ,  $N_{24,26} = 0.174$ ,  $N_{25,25} = 0.010$ ,  $N_{25,26} = 0.022$  and  $N_{26,26} = 0.012$ .

To record spectra of the  $A \leftarrow X$  transition of  $\text{Mg}_2$ , the  $\text{Mg}_2^+$  ions produced by  $(1 + 1')$  resonance-enhanced multiphoton ionization (REMPI) are extracted using a single large electric-field pulse of  $+240$   $\text{V cm}^{-1}$ . The ion signals corresponding to the different  $\text{Mg}_2^+$  isotopomers are monitored as a function of the wavenumber of the doubled output of Laser 1. To record PFI-ZEKE-PE spectra, the wavenumber of Laser 1 is kept fixed so as to select a specific rovibrational level of the A state. The doubled wavenumber of Laser 2 is scanned across the  $X^+ \leftarrow A$  ionization thresholds while monitoring the yield of electrons generated by delayed pulsed field ion-

ization of very high Rydberg states (principal quantum number  $\gtrsim 200$ ) located just below the successive ionization thresholds [52]. Sequences of small electric-field pulses are applied to the stack to field ionize the Rydberg states and accelerate the electrons towards the detector. The number of pulses in the sequence, their amplitudes, and their polarities determine the resolution of the PFI-ZEKE-PE spectra and the signal strength [53]. After systematic optimization, we found that the sequences (0.09, -0.09, -0.17, -0.26, -0.35, -0.43, -0.52) V cm<sup>-1</sup> and (0.17, -0.12, -0.21, -0.29, -0.36) V cm<sup>-1</sup> provided the best spectra for weak and strong bands of the photoelectron spectrum, respectively, resulting in spectral resolutions of 0.5 and 0.6 cm<sup>-1</sup>, respectively.

The lines recorded in PFI-ZEKE-PE spectra correspond to high Rydberg states of the neutral molecule located just below the ionization thresholds associated with specific rovibronic levels of the molecular ion. To determine the position of the field-free ionization thresholds, the spectra were corrected for these field-induced shifts following the procedure described in Refs. [53, 54]. We verified the accuracy of the correction procedure by recording the PFI-ZEKE-PE spectrum of metastable Mg(3s3p <sup>3</sup>P<sub>1</sub>) atoms produced in the source. The ionization energy of this state is well known (39800.59(4) cm<sup>-1</sup> [55]), and we found that the correction of the field-induced shifts is accurate to within 0.04 cm<sup>-1</sup>, a value more than 10 times smaller than the full width at half maximum of the lines of the photoelectron spectra ( $\sim 0.5$  cm<sup>-1</sup>).

### III. RESULTS

#### A. (1 + 1') REMPI spectra of the A ← X transition of Mg<sub>2</sub>

The ground-state Mg<sub>2</sub> molecules produced in the experiment were characterized by recording (1 + 1') REMPI spectra of the A ← X transition. A typical spectrum is shown in Fig. 2 and corresponds to the A <sup>1</sup>Σ<sub>u</sub><sup>+</sup>(v' = 10) ← X <sup>1</sup>Σ<sub>g</sub><sup>+</sup>(v'' = 0) vibrational band.

The X <sup>1</sup>Σ<sub>g</sub><sup>+</sup> and A <sup>1</sup>Σ<sub>u</sub><sup>+</sup> states are well described by Hund's angular-momentum-coupling case (b), with N'' and N' representing the total-angular-momentum-without-spin quantum numbers of the initial and final states, respectively. Each vibrational band of this Σ – Σ transition thus consists of P (ΔN = N' – N'' = -1) and R (ΔN = 1) rotational branches. Because of nuclear-spin statistics, the homonuclear Mg<sub>2</sub> isotopomers with zero nuclear spin (<sup>24</sup>Mg<sub>2</sub> and <sup>26</sup>Mg<sub>2</sub>) can only occupy rotational levels of even values of N for gerade electronic states and odd values of N for ungerade electronic states. This property can be clearly seen in Fig. 3, which shows the spectra of the A <sup>1</sup>Σ<sub>u</sub><sup>+</sup>(v' = 10) ← X <sup>1</sup>Σ<sub>g</sub><sup>+</sup>(v'' = 0) transition for all Mg<sub>2</sub> isotopomers, and where every second spectral line is missing for the <sup>24</sup>Mg<sub>2</sub> and <sup>26</sup>Mg<sub>2</sub> species. The rotational structure of the band of the

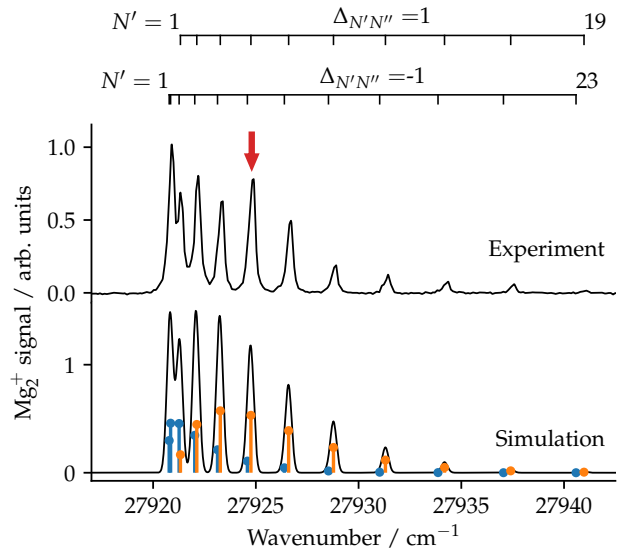


FIG. 2. Measured (top) and calculated (bottom) REMPI spectra of the A <sup>1</sup>Σ<sub>u</sub><sup>+</sup>(v' = 10) ← X <sup>1</sup>Σ<sub>g</sub><sup>+</sup>(v'' = 0) transition of <sup>24</sup>Mg<sup>24</sup>Mg. The assignment bars above the spectra give the positions of transitions to rotational levels of the A <sup>1</sup>Σ<sub>u</sub><sup>+</sup>(v' = 10) state of successive value of N'. The stick spectrum in the lower panel shows the wavenumbers and relative intensities of individual rovibronic transitions for a rotational temperature of 7 K. The vertical arrow indicates the wavenumber at which the first laser was set when recording the PFI-ZEKE-PE spectra presented in Fig. 4.

homonuclear <sup>25</sup>Mg<sub>2</sub> molecule (*I*<sub>25Mg</sub> = 5/2) cannot be unambiguously observed in the spectra because it possesses the same mass and approximately the same isotopic shift as the <sup>24</sup>Mg<sup>26</sup>Mg isotopomer while its natural abundance is more than 10 times smaller. When taking laser-pulse-energy variations across the spectral range into account, the amplitudes of the spectra match the relative natural abundances of the various isotopomers.

The REMPI spectra were modelled using band origins and rotational constants calculated with the accurate potential-energy functions of the X <sup>1</sup>Σ<sub>g</sub><sup>+</sup> and A <sup>1</sup>Σ<sub>u</sub><sup>+</sup> electronic states determined from high-resolution spectroscopic data by Knöckel *et al.* [2, 18]. At the low rotational temperature of the supersonic expansion, only rotational levels with N'' ≤ 24 are occupied and centrifugal distortion effects are negligible within the experimental accuracy. The agreement between the observed and calculated line positions is excellent. The line intensities of the individual A <sup>1</sup>Σ<sub>u</sub><sup>+</sup>(v', N') ← X <sup>1</sup>Σ<sub>g</sub><sup>+</sup>(v'', N'') transitions were calculated from the line strengths for transitions between states described by Hund's angular-momentum-coupling case (b) [56]. Rotational levels of the X(v = 0) initial state were assumed to be thermally populated, and the theoretical spectrum matched the experimental one best for a rotational temperature of

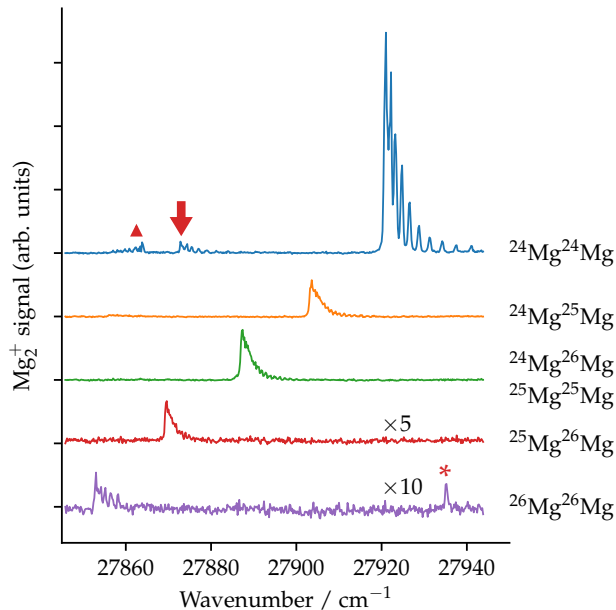


FIG. 3. Spectra of the  $A\ ^1\Sigma_u^+(v' = 10) \leftarrow X\ ^1\Sigma_g^+(v'' = 0)$  transition of the different isotopomers of  $Mg_2$ , as labeled on the right of the figure. The vertical arrow shows the position of the  $A\ ^1\Sigma_u^+(v' = 10) \leftarrow X\ ^1\Sigma_g^+(v'' = 1)$  hot band for  $^{24}Mg_2$ . The line labeled with an asterisk could not be assigned. The band marked by a triangle is tentatively assigned to excitation from the  $(1)\ ^3\Sigma_u^+$  state to a high-lying excited state (see text). The vertical scales of the spectra of  $^{25}Mg^{26}Mg$  and  $^{26}Mg_2$  are magnified by a factor 5 and 10, respectively, for visibility.

$\sim 7$  K. The vibrational temperature of the ground-state molecules in the beam was derived from the relative amplitudes of the  $A\ ^1\Sigma_u^+(v') \leftarrow X\ ^1\Sigma_g^+(0)$  band and the  $A\ ^1\Sigma_u^+(v') \leftarrow X\ ^1\Sigma_g^+(1)$  hot band (see Fig. 3 for the  $^{24}Mg_2$  isotopomer) taking into account the associated Franck-Condon factors calculated using the potential-energy functions from Refs. [2, 18]. The resulting value of  $\sim 30$  K indicates that the cooling of the vibrational degree of freedom in the supersonic expansion is less efficient than the cooling of the rotational ones.

The band marked by a triangle in Fig. 3 does not correspond to the  $A\ ^1\Sigma_u^+(v') \leftarrow X\ ^1\Sigma_g^+(v'')$  band system. Unlike the other bands we recorded, it degrades to lower wavenumbers, rather than to higher wavenumbers. Consequently, the rotational constant of the upper state is smaller, and its mean internuclear distance larger, than in the initial state. In the wavenumber range considered, no other electronic state can be reached by dipole excitation from the  $X\ ^1\Sigma_g^+(v'' \leq 4)$  levels. In particular, the  $(1)\ ^1\Pi_u$  state investigated in Refs. [18, 22] is not accessible energetically. Transitions from the ground state to triplet states cannot give rise to the observed band either, because only the dissociation continua of the low-lying triplet states of  $Mg_2$  correlating to the  $Mg(3s^2\ ^1S) + Mg(3s3p\ ^3P)$  dissociation asymptote are

accessible at the photon energies used to record the spectra.

Metastable molecules are known to form in laser-ablation supersonic-expansion sources, an example being the production of  $MgAr$  molecules in their  $a\ ^3\Pi_0$  state [57].  $Mg_2$  molecules in metastable states may be formed in our experiment, in particular the low-lying  $(1)\ ^3\Pi_g$  and  $(1)\ ^3\Sigma_u^+$  states correlating to the  $Mg(3s^2\ ^1S) + Mg(3s3p\ ^3P)$  dissociation asymptote and the  $(1)\ ^1\Pi_g$  state correlating to the  $Mg(3s^2\ ^1S) + Mg(3s3p\ ^1P)$  dissociation asymptote (see, *e.g.*, Ref. [58]). Fluorescence of the  $^1\Pi_g$  and  $^3\Pi_g$  states to the  $X\ ^1\Sigma_g^+$  ground state is forbidden because of the  $g \leftrightarrow u$  selection rule whereas fluorescence of the  $^3\Sigma_u^+$  state is forbidden by the approximate  $\Delta S = 0$  selection rule. The  $(1)\ ^3\Sigma_u^+$  state can in principle radiate to the ground state *via* spin-orbit mixing with  $^1\Pi_u$  states, but its radiative lifetime is not known. *Ab initio* calculations predict that these three states are the lowest-lying states of their respective electronic symmetries and that they are strongly bound [58].

Because of nuclear-spin symmetry, only odd values of  $N''$  are allowed for the  $^3\Sigma_u^+$  state whereas both even and odd values of  $N''$  can be populated in the case of the  $^1,^3\Pi_g$  states. We have observed in Fig. 3 that the existence of both even and odd  $N''$  values in the initial state leads to unresolved rotational structures of the bands whereas the rotational structure is partially resolved when only even (odd) values are allowed (compare, for example, the spectra of the  $^{24}Mg^{25}Mg$  and  $^{24}Mg_2$  isotopomers). Because the rotational structure of the band marked by a triangle in Fig. 3 is partially resolved, we tentatively attribute it to excitation of metastable  $^{24}Mg_2$  molecules from the  $(1)\ ^3\Sigma_u^+$  state to a  $^3\Sigma_g^+$  or  $^3\Pi_g$  state in the dense manifold of excited states lying  $\sim 12000\text{ cm}^{-1}$  below the  $Mg_2^+ X^+$  ionization threshold. This tentative assignment is further supported by the fact that similar transitions were observed in  $Be_2$  molecules produced in a laser-ablation supersonic-expansion source [59]. Specifically, transitions from the  $(1)\ ^3\Sigma_u^+$  state of  $Be_2$  to the  $(2)\ ^3\Pi_g$  and  $(3)\ ^3\Pi_g$  state were observed by REMPI spectroscopy in the same photon-energy range as the  $B\ ^1\Sigma_u^+ \leftarrow X\ ^1\Sigma_g^+$  and  $A\ ^1\Pi_u \leftarrow X\ ^1\Sigma_g^+$  transitions of  $Be_2$  [59]. Further investigations are required to clarify the assignment of this weak band.

## B. PFI-ZEKE-PE spectra of the $X^+ \leftarrow A$ photoionizing transition of $Mg_2$

PFI-ZEKE-PE spectra of the  $X^+ \ ^2\Sigma_u^+(v^+, N^+) \leftarrow A\ ^1\Sigma_u^+(v', N')$  photoionizing transitions of the  $^{24}Mg_2$  isotopomer were recorded for  $v^+$  in the range from 3 to 14. For each value of  $v^+$ ,  $v'$  was chosen so that the Franck-Condon factor of the transition was sufficiently large to record spectra with good signal-to-noise ratios. The spectra of the  $v^+ = 9 \leftarrow v' = 10$  and  $v^+ = 10 \leftarrow v' = 10$  transitions are presented as examples in Fig. 4.

In the experiment,  $Mg_2$  in its ground electronic

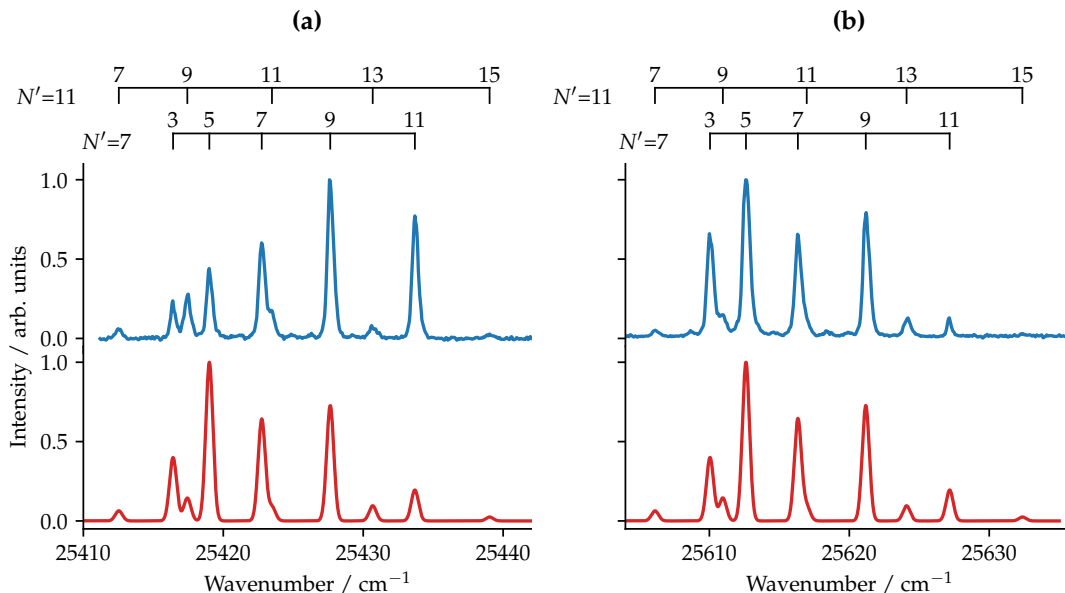


FIG. 4. Measured (top) and calculated (bottom) PFI-ZEKE photoelectron spectra of (a) the  $X^+ \ ^2\Sigma_u^+(v^+ = 9) \leftarrow A \ ^1\Sigma_u^+(v' = 10)$  and (b) the  $X^+ \ ^2\Sigma_u^+(v^+ = 10) \leftarrow A \ ^1\Sigma_u^+(v' = 10)$  photoionizing transitions of  $^{24}\text{Mg}_2$ . The assignment bars indicate transitions from initial rotational states with  $N' = 7$  and  $11$  to states of the ion with successive values of  $N^+$ . The dominant branches correspond to  $N^+ - N' = 0, \pm 2, \pm 4$ .

and vibrational state was first photoexcited to selected  $A \ ^1\Sigma_u^+(v', N')$  rovibrational states. An example is illustrated by the red arrow in Fig. 2, which indicates the wavenumber at which the first laser ( $\tilde{\nu}_1 = 27924.8 \text{ cm}^{-1}$ ) excites ground-state molecules with  $v'' = 0$  and  $N'' = 6, 12$  to levels of the A state with  $v' = 10$  and  $N' = 7$  and  $11$ , respectively. PFI-ZEKE-PE spectra were then recorded from these two levels by scanning the wavenumber of Laser 2 in a range just below the  $X^+ \ ^2\Sigma_u^+(v^+ = 9 - 10, N^+)$  ionization thresholds. The spectra associated with each electric-field pulse of the PFI sequence were corrected for the field-induced shifts, as described in Sec. II, and summed to yield the spectra depicted in the top panels of Fig. 4.

These spectra exhibit more rotational branches than the P ( $\Delta N = -1$ ) and R ( $\Delta N = +1$ ) branches characteristic of  $\Sigma - \Sigma$  transitions between bound states. This observation originates from the fact that the photoelectron also carries angular momentum, which needs to be considered when deriving photoionization selection rules [60–62]. The photoelectron is described as a superposition of partial waves with angular-momentum quantum numbers  $l$ . The parity of the final-state wavefunction is determined by the  $g/u$  symmetry of the ion core, which is ungerade in the present case, the parity of the Rydberg electron, which is given by  $(-1)^l$ , and the parity of the ion-core rotational function, which is  $(-1)^{N^+}$ . The transitions must obey the rovibronic parity selection

rule [60–62]

$$\pm \leftrightarrow \pm \quad \text{for } l \text{ odd}, \quad (1)$$

$$\pm \leftrightarrow \mp \quad \text{for } l \text{ even}, \quad (2)$$

where the  $\pm$  signs give the rovibronic parity of the neutral and ionized molecules. Because both the A state of  $\text{Mg}_2$  and the  $X^+$  state of  $\text{Mg}_2^+$  have  $u$  electronic symmetry, the rotational selection rule can be expressed as

$$\Delta N = N^+ - N' = 0, \pm 2, \pm 4, \dots \quad \text{for } l \text{ odd}, \quad (3)$$

$$\Delta N = \pm 1, \pm 3, \pm 5, \dots \quad \text{for } l \text{ even}. \quad (4)$$

Upon photoionization, an electron is removed from the  $3p\sigma_g$  orbital of the A state with electronic configuration  $(3s\sigma_g)^2(3s\sigma_u^*)^1(3p\sigma_g)^1$ . Consequently, the photoelectron partial waves must have an odd  $l$  value, and  $\Delta N$  must be even.

For the homonuclear isotopomers, the parity selection rule gives the same result as the nuclear-spin-symmetry conservation rule. Rotational levels of  $^{24}\text{Mg}_2$  and  $^{26}\text{Mg}_2$  ( $I_{^{24}\text{Mg}} = I_{^{26}\text{Mg}} = 0$ ) of ortho nuclear-spin symmetry correspond to odd- $N$  levels in the A and  $X^+$  states, so that  $\Delta N$  must be even. Rotational levels of  $^{25}\text{Mg}_2$  ( $I_{^{25}\text{Mg}} = 5/2$ ) of ortho (para) nuclear-spin symmetry have statistical weights 21 (15) and correspond to even- $N$  (odd- $N$ ) levels in the A and  $X^+$  states. For the heteronuclear isotopomers, there are no restrictions from the conservation of nuclear-spin symmetry, and the  $g/u$  symmetry is only approximate. We have, however, observed no evidence of such a symmetry breaking in the experimental spectra we recorded.

The most intense lines in the experimental spectra are well described by 5 rotational branches corresponding to  $N^+ - N' = \pm 0, \pm 2, \pm 4$ , as shown by the assignment bars in Fig. 4. The line positions were determined from the experimental spectra from fits using Gaussian functions. The band origins  $\tilde{\nu}_{v^+v'}$  and the rotational constants  $B_{v^+}$  of the final states were then obtained from the line positions in a least-squares fit based on the standard expression [63]

$$\tilde{\nu} = \tilde{\nu}_{v^+v'} + B_{v^+} N^+ (N^+ + 1) - B_{v'} N' (N' + 1). \quad (5)$$

$$\sigma_{N^+ \leftarrow N'} \propto \sum_{l'=\lambda'}^{\infty} \frac{2N^+ + 1}{2l' + 1} \begin{pmatrix} N^+ & l' & N' \\ -\Lambda^+ & \lambda' & \Lambda' \end{pmatrix}^2 |c_{l'}|^2 \left[ l' \left| F_{\alpha, l'}^{E, l' - 1} \right|^2 + (l' + 1) \left| F_{\alpha, l'}^{E, l' + 1} \right|^2 \right]. \quad (6)$$

In Eq. (6), the quantum number  $\lambda'$  is the projection on the molecular axis of the orbital angular momentum  $l'$  associated with the single-center expansion of the bound molecular orbital. The coefficients of the single-center expansion are represented by  $|c_{l'}|^2$  and the quantities  $F_{\alpha, l'}^{E, l'}$  are bound-free radial transition integrals. Here, we assume that, as in the hydrogen atom,  $\left| F_{\alpha, l'}^{E, l' + 1} \right|^2 \gg \left| F_{\alpha, l'}^{E, l' - 1} \right|^2$ , such that the first term of the expression enclosed between the square brackets on the right hand side of Eq. (6) can be neglected. The dependence of  $\left| F_{\alpha, l'}^{E, l' + 1} \right|^2$  on the energy is assumed to be negligible within the range probed in the experiment.

The lower panels of Fig. 4 show the spectra of the  $X^+ \ ^2\Sigma_u^+(9) \leftarrow A \ ^1\Sigma_u^+(10)$  (left) and  $X^+ \ ^2\Sigma_u^+(10) \leftarrow A \ ^1\Sigma_u^+(10)$  (right) transitions calculated using the results of a fit based on Eq. (5) and the expression for the line intensities given by Eq. (6). In the latter equation, the single-center expansion was truncated to  $l' \leq 4$  ( $l'$  even), which yields the 5 rotational branches observed in the experimental spectrum. The coefficients  $\left| c_{l'} F_{\alpha, l'}^{E, l' + 1} \right|^2 = |b_{l'}|^2$  were manually adjusted to reproduce as well as possible the line intensities of the entire set of PFI-ZEKE-PE spectra we recorded, yielding  $|b_0|^2 = 0.09$ ,  $|b_2|^2 = 0.57$  and  $|b_4|^2 = 0.34$ . The populations of the initial rotational states ( $N' = 7, 11$ ) were determined from the calculated line intensities of the respective  $A \ ^1\Sigma_u^+(v', N') \leftarrow X \ ^1\Sigma_g^+(v'', N'')$  transitions (vertical bars in the lower panel of Fig. 2).

The experimental line intensities are well reproduced by the calculation in the case of the  $X^+ \ ^2\Sigma_u^+(10) \leftarrow A \ ^1\Sigma_u^+(10)$  transition (right column in Fig. 4), but the agreement is significantly worse for the  $X^+ \ ^2\Sigma_u^+(9) \leftarrow A \ ^1\Sigma_u^+(10)$  transition (left column). Equation (6) assumes that direct photoionization is predominant and disregards any interaction between the various ionization

The rotational constant  $B_{v'}$  of the A state was fixed to the value obtained from the potential-energy function of Ref. 18. The values obtained from the fit are listed in Table I.

The intensities of the various  $X^+ \ ^2\Sigma_u^+(v^+, N^+) \leftarrow A \ ^1\Sigma_u^+(v', N')$  ionizing transitions can be estimated using a model developed by Buckingham, Orr and Sichel [64] (see also Ref. 65). The model relies on a single-center expansion of the molecular orbital describing the bound electron before photoionization, from which the following expression for the photoionization cross section can be derived:

channels. Such interactions couple ionization channels associated with different ion-core rovibrational states and different photoelectron orbital-angular momenta and energies, and give rise to phenomena such as vibrational and rotational autoionization. Channel interactions can significantly affect the rotational line intensities observed in PFI-ZEKE-PE spectra [65]. Because the transition dipole moment scales as  $n^{-3/2}$  ( $n$  is the principal quantum number), the coupling of Rydberg states with different  $n$  values modifies the photoexcitation probability.

In the spectra we measured, strong deviations of the line intensities from the predictions of Eq. (6) are observed for  $v^+ = 3 - 9, 12, 14$ . The intensities of the lines with positive  $N^+ - N'$  values are systematically underestimated. When the effects of interactions between different rotational channels, *i.e.*, channels of different  $N^+$  values, are significant, the intensities of the rotational branches with  $N^+ - N' > 0$  are expected to be reduced and those with  $N^+ - N' < 0$  to be enhanced [65], which is the opposite of what is observed in the present case. Because the first electronically excited state of  $Mg_2^+$  lies more than  $16\,000 \text{ cm}^{-1}$  above the ground state [27], electronic channel interactions do not play a role. Consequently, we attribute the observed deviations of the rotational line intensities from the model predictions to vibrational channel interactions.

The values of the band origins  $\tilde{\nu}_{v^+v'}$  and rotational constants  $B_{v^+}$  of the  $X^+(v^+)$  levels listed in Table I were obtained from least-squares fits based on the line positions derived from the spectra we measured. The statistical uncertainty of the band origins was taken as the standard deviation of the values determined from spectra of the same vibrational band ( $v^+ = 13 \leftarrow v' = 10$ ) recorded for different initial rotational states ( $N' = 5, 7$ ). The statistical uncertainties of the values of the rotational constants were taken as the  $1\sigma$  uncertainties of the corresponding fits based on Eq. (5). In cases where the  $1\sigma$  value was less than  $5 \times 10^{-4} \text{ cm}^{-1}$ , the standard

TABLE I. Band origins  $\tilde{\nu}_{v^+v'}$  of the  $X^+ \ ^2\Sigma_u^+(v^+) \leftarrow A \ ^1\Sigma_u^+(v')$  ionizing transitions of  $^{24}\text{Mg}_2$ , term values  $T_{v^+}$  of the  $X^+ \ ^2\Sigma_u^+(v^+)$  vibrational levels relative to the ground rovibronic state of  $^{24}\text{Mg}_2$  ( $X \ ^1\Sigma_g^+(v'' = 0)$ ) and rotational constants  $B_{v^+}^+$  of the  $X^+ \ ^2\Sigma_u^+(v^+)$  levels of  $^{24}\text{Mg}_2^+$ . All values are in  $\text{cm}^{-1}$ . The numbers in parentheses represent one standard deviation in units of the last digit. Values in italics are for the  $^{24}\text{Mg}^{26}\text{Mg}$  isotopomer.

$v'$	$v^+$	$\tilde{\nu}_{v^+v'}$	$T_{v^+}$	$B_{v^+}^+$
5	3	25078.58(10)	52136.52(10)	0.1513(15)
5	4	25284.96(10)	52342.90(10)	0.150(2)
		<i>25285.6(5)</i>	<i>52325.0(5)</i>	–
7	5	25137.53(10)	52547.36(10)	0.1496(15)
7	6	25339.64(10)	52749.47(10)	0.1483(9)
10	7	25028.56(10)	52949.62(10)	0.1461(5)
10	8	25226.46(10)	53147.52(10)	0.1453(5)
10	9	25422.21(10)	53343.27(10)	0.1440(5)
10	10	25615.86(10)	53536.92(10)	0.1427(5)
10	11	25807.46(10)	53728.52(10)	0.1414(9)
10	12	25996.97(10)	53918.03(10)	0.1409(5)
10	13	26184.22(6)	54105.28(6)	0.1387(5)
		<i>26169.42(5)</i>	<i>54540.41(6)</i>	<i>0.1358(11)</i>
10	14	26369.64(10)	54290.70(10)	0.1386(5)

deviation of the rotational constants determined from the spectra of the  $v^+ = 13 \leftarrow v' = 10$  band ( $0.0005 \text{ cm}^{-1}$ ) was taken instead. The statistical uncertainties of the band origins and rotational constants obtained from the spectra of the  $v^+ = 13 \leftarrow v' = 10$  bands of the  $^{24}\text{Mg}_2$  and  $^{24}\text{Mg}^{26}\text{Mg}$  isotopomers for different  $N'$  values were taken as the standard deviation of the mean.

Term values of the  $X^+ \ ^2\Sigma_u^+(v^+)$  vibrational levels relative to the  $X \ ^1\Sigma_g^+(v'' = 0)$  ground state of the neutral molecule were determined using the term values of the  $A \ ^1\Sigma_u^+(v')$  levels calculated using the potential-energy function of Ref. 18. The mean precision of  $0.025 \text{ cm}^{-1}$  stated by the authors of [18] was taken as the uncertainty of these A-state term values.

The absolute assignment of the vibrational quantum numbers of the  $X^+(v^+)$  levels was obtained in a standard analysis of the isotopic shifts [63] from spectra of the  $X^+ \ ^2\Sigma_u^+(13) \leftarrow A \ ^1\Sigma_u^+(10)$  and  $X^+ \ ^2\Sigma_u^+(4) \leftarrow A \ ^1\Sigma_u^+(5)$  transitions recorded for the  $^{24}\text{Mg}_2$  and  $^{24}\text{Mg}^{26}\text{Mg}$  isotopomers.

### C. Molecular constants

Molecular constants characterizing the  $X^+ \ ^2\Sigma_u^+$  ground electronic state of  $\text{Mg}_2^+$  were derived from the term values and rotational constants obtained in this work (see Table I) and are listed in Table II. The harmonic ( $\omega_e$ ) and

anharmonic ( $\omega_e x_e, \omega_e y_e$ ) vibrational constants of  $^{24}\text{Mg}_2^+$  were obtained in a least-squares fit based on the standard polynomial expansion [63]

$$T_{v^+} = T_e + \omega_e \left( v^+ + \frac{1}{2} \right) - \omega_e x_e \left( v^+ + \frac{1}{2} \right)^2 \quad (7)$$

$$+ \omega_e y_e \left( v^+ + \frac{1}{2} \right)^3. \quad (8)$$

The adiabatic ionization energy  $E_I$  of  $^{24}\text{Mg}_2$  ( $X \ ^1\Sigma_g^+(v'' = 0)$ ) corresponds to  $\frac{E_I}{hc} = T_{v^+=0} = 51\,503.9(4) \text{ cm}^{-1}$ . The equilibrium rotational constant  $B_e$  and rotation-vibration coupling constant  $\alpha_e$  were obtained from the rotational constants in a least-squares fit based on the standard expression [63]

$$B_{v^+}^+ = B_e - \alpha_e \left( v^+ + \frac{1}{2} \right). \quad (9)$$

Finally, the dissociation energy  $D_0(X^+)$  of the  $X^+ \ ^2\Sigma_u^+$  state was determined to be  $10\,572.3(6) \text{ cm}^{-1}$  from the thermodynamic cycle

$$D_0(X^+) = E_I(\text{Mg}) + D_0(X) - E_I, \quad (10)$$

using the dissociation energy of the  $X \ ^1\Sigma_g^+$  state of  $^{24}\text{Mg}_2$  reported by Knöckel *et al.* [2] ( $D_0(X)/(hc) = 405.1(5) \text{ cm}^{-1}$ ) and the ionization energy of  $^{24}\text{Mg}$  ( $E_I(\text{Mg})/(hc) = 61671.05(3) \text{ cm}^{-1}$  [5, 55]).

The present value of the dissociation energy is in agreement with, but 500 times more accurate than, the only other experimental value we could find in the literature ( $10\,200(300) \text{ cm}^{-1}$  [25]). Molecular constants from recent *ab initio* calculations [5, 27, 29, 30] are consistent with the present values (see Table II for a detailed comparison with the results of Refs. [5, 30]). Recent high-level *ab initio* calculations based on the procedure used to characterize the ground and excited states of the  $\text{Sr}_2^+$  ion [31] also yield values ( $D_e = 10667 \text{ cm}^{-1}$  and  $R_e = 5.694 a_0$  [66]) that are in excellent agreement with our experimental values.

## IV. CONCLUSIONS

We reported an experimental study of the  $X^+ \ ^2\Sigma_u^+$  electronic ground state of the  $\text{Mg}_2^+$  ion. Neutral  $\text{Mg}_2$  molecules in their ground  $X \ ^1\Sigma_g^+(v'' = 0)$  vibronic state were produced in a laser-ablation supersonic-expansion source and excited to high Rydberg states below the  $X^+(v^+, N^+)$  ionization thresholds by resonant  $(1 + 1')$  two-photon absorption. The PFI-ZEKE-PE spectra of the  $v^+ = 3 - 14$  vibrational levels of the ground state ion were recorded with rotational resolution. Deviations of the line intensities from those predicted for direct photoionization were observed and attributed to vibrational channel interactions. Term values and rotational

TABLE II. Comparison of the molecular constants of the  $X^+ \ ^2\Sigma_u^+$  ground electronic state of  $^{24}\text{Mg}_2^+$  derived from the PFI-ZEKE-PE spectra with values obtained in *ab initio* quantum chemical calculations [5, 30]. The molecular constants are in  $\text{cm}^{-1}$  except  $R_e$  which is in Bohr radii ( $a_0$ ). The numbers in parentheses represent one standard deviation in units of the last digit.

	Present	Ref. 30	Ref. 5
$E_1/(hc)$	51 503.9(4)		
$D_0(X^+)$	10 572.3(6)		
$D_e(X^+)$	10 679.6(6) <sup>a</sup>	10 575 <sup>b</sup>	10 642
$\omega_e$	215.25(14)	215	215.49
$\omega_e x_e$	1.102(16)		0.59
$\omega_e y_e$	0.0015(6)		
$R_e$	5.684(9)	5.70	5.69
$B_e$	0.1554(5)	0.154	0.155
$\alpha_e$	0.001 20(5)		0.0011

<sup>a</sup> Estimated using  $D_e = D_0 + \omega_e/2 - \omega_e x_e/4 + \omega_e y_e/8$

<sup>b</sup> The potential-well depth of  $10532 \text{ cm}^{-1}$  reported in Ref. [30] is a misprint [66].

constants were extracted from the spectra and a set of accurate molecular constants was derived. In particular, the present work provides improved values of the adiabatic ionization energy of  $^{24}\text{Mg}_2$  ( $51\,503.9(4) \text{ cm}^{-1}$ ) and of the ground-state dissociation energy of  $^{24}\text{Mg}_2^+$  ( $10\,572.3(6) \text{ cm}^{-1}$ ). The experimental [25] and theoretical [5, 27, 29, 30, 66] data available in the literature are consistent with the present results. Finally, a band observed in the  $(1+1')$  REMPI spectrum of the  $A \ ^1\Sigma_u^+(v' = 10) \leftarrow X \ ^1\Sigma_g^+(v'' = 0)$  transition could not be assigned

to any multiphoton ionization process from ground-state  $\text{Mg}_2$  molecules and was tentatively attributed instead to a transition from metastable molecules in the  $(1) \ ^3\Sigma_u^+$  state.

The present work opens the possibility to study electronically excited states of  $\text{Mg}_2^+$ , and in particular its Rydberg states, by isolated-core multiphoton Rydberg dissociation [37]. The structure and dynamics of these states are expected to differ from the Rydberg states of  $\text{MgAr}^+$ , which is one of the few molecular ions for which the Rydberg states are well characterized [38–42]. In the case of  $\text{MgAr}^+$ , the ground state of the doubly charged ion ( $\text{MgAr}^{2+}$ ) to which the Rydberg series converge is thermodynamically stable [42]. In contrast, the electronic ground state of  $\text{Mg}_2^{2+}$  is unstable overall, and a local minimum in the Coulomb-repulsion-type potential-energy function is predicted to support several metastable vibrational states [36]. Rydberg series of  $\text{Mg}_2^+$  converging to these metastable  $\text{Mg}_2^{2+}$  levels should exhibit potential-energy functions and dynamical properties very different from those of  $\text{MgAr}^+$ , and their systematic investigation is a perspective of future work.

## V. ACKNOWLEDGEMENTS

We thank M. Tomza and D. Reich and C. Koch for providing us the data files of the potential-energy functions they calculated for  $\text{Mg}_2^+$  and  $\text{Mg}_2$ , respectively. We also thank H. Knöckel and E. Tiemann for assistance in using the potential-energy functions they derived for the X and A state of  $\text{Mg}_2$ . Finally, we thank Hansjürg Schmutz and Josef A. Agner for their technical assistance. This work is supported financially by the Swiss National Science Foundation (Grant No. 200020B–200478) and the European Research Council through an ERC advanced grant (Grant No. 743121) under the European Union’s Horizon 2020 research and innovation programme.

- 
- [1] O. Allard, A. Pashov, H. Knöckel, E. Tiemann, Ground-state potential of the Ca dimer from Fourier-transform spectroscopy, *Phys. Rev. A* 66 (4) (2002) 042503. doi:10.1103/PhysRevA.66.042503.
- [2] H. Knöckel, S. Rühmann, E. Tiemann, The  $X \ ^1\Sigma_g^+$  ground state of  $\text{Mg}_2$  studied by Fourier-transform spectroscopy, *J. Chem. Phys.* 138 (9) (2013) 094303. doi:10.1063/1.4792725.
- [3] M. C. Heaven, J. M. Merritt, V. E. Bondybey, Bonding in beryllium clusters, *Annu. Rev. Phys. Chem.* 62 (1) (2011) 375–393. doi:10.1146/annurev-physchem-032210-102545.
- [4] A. Stein, H. Knöckel, E. Tiemann, Fourier-transform spectroscopy of  $\text{Sr}_2$  and revised ground-state potential, *Phys. Rev. A* 78 (4) (2008) 042508. doi:10.1103/PhysRevA.78.042508.
- [5] H. Li, H. Feng, W. Sun, Y. Zhang, Q. Fan, K. A. Peterson, Y. Xie, H. F. Schaefer III, The alkaline earth dimer cations ( $\text{Be}_2^+$ ,  $\text{Mg}_2^+$ ,  $\text{Ca}_2^+$ ,  $\text{Sr}_2^+$ , and  $\text{Ba}_2^+$ ). Coupled cluster and full configuration interaction studies, *Mol. Phys.* 111 (14-15) (2013) 2292–2298. doi:10.1080/00268976.2013.802818.
- [6] I. Røeggen, J. Almlöf, Interatomic potential for the  $X \ ^1\Sigma_g^+$  state of  $\text{Be}_2$ , *Int. J. Quantum Chem.* 60 (1) (1996) 453–466. doi:10.1002/(SICI)1097-461X(1996)60:1<453::AID-QUA44>3.0.CO;2-A.
- [7] V. E. Bondybey, J. H. English, Laser vaporization of beryllium: Gas phase spectrum and molecular potential of  $\text{Be}_2$ , *J. Chem. Phys.* 80 (1) (1984) 568–570. doi:10.1063/1.446434.
- [8] J. M. Merritt, V. E. Bondybey, M. C. Heaven, Beryllium dimer—caught in the act of bonding, *Science* 324 (5934) (2009) 1548–1551. doi:10.1126/science.1174326.
- [9] T. K. T. Kurosu, F. S. F. Shimizu, Laser cooling and trapping of alkaline earth atoms, *Jpn. J. Appl. Phys.* 31 (3R) (1992) 908. doi:10.1143/JJAP.31.908.

- [10] N. Beverini, F. Giammanco, E. Maccioni, F. Strumia, G. Vissani, Measurement of the calcium  $^1P_1 - ^1D_2$  transition rate in a laser-cooled atomic beam, *J. Opt. Soc. Am. B* 6 (11) (1989) 2188. doi:10.1364/JOSAB.6.002188.
- [11] X. Xu, T. H. Loftus, J. L. Hall, A. Gallagher, J. Ye, Cooling and trapping of atomic strontium, *J. Opt. Soc. Am. B* 20 (5) (2003) 968. doi:10.1364/JOSAB.20.000968.
- [12] W. Neuhauser, M. Hohenstatt, P. Toschek, H. Dehmelt, Optical-sideband cooling of visible atom cloud confined in parabolic well, *Phys. Rev. Lett.* 41 (4) (1978) 233–236. doi:10.1103/PhysRevLett.41.233.
- [13] D. J. Wineland, R. E. Drullinger, F. L. Walls, Radiation-pressure cooling of bound resonant absorbers, *Phys. Rev. Lett.* 40 (25) (1978) 1639–1642. doi:10.1103/PhysRevLett.40.1639.
- [14] E. Tiesinga, S. Kotochigova, P. S. Julienne, Scattering length of the ground-state Mg + Mg collision, *Phys. Rev. A* 65 (4) (2002) 042722. doi:10.1103/PhysRevA.65.042722.
- [15] S. B. Nagel, P. G. Mickelson, A. D. Saenz, Y. N. Martinez, Y. C. Chen, T. C. Killian, P. Pellegrini, R. Côté, Photoassociative spectroscopy at long range in ultracold strontium, *Phys. Rev. Lett.* 94 (8) (2005) 083004. doi:10.1103/PhysRevLett.94.083004.
- [16] G. Zimmer, T. Binnewies, F. Riehle, E. Tiemann, Photoassociation of cold Ca atoms, *Phys. Rev. Lett.* 85 (11) (2000) 4.
- [17] K. M. Jones, E. Tiesinga, P. D. Lett, P. S. Julienne, Ultracold photoassociation spectroscopy: Long-range molecules and atomic scattering, *Rev. Mod. Phys.* 78 (2) (2006) 483–535. doi:10.1103/RevModPhys.78.483.
- [18] H. Knöckel, S. Rühmann, E. Tiemann, The  $A^2\Sigma_u^+$  system of  $Mg_2$ , *Eur. Phys. J. D* 68 (10) (2014) 293. doi:10.1140/epjd/e2014-50289-9.
- [19] H. Scheingraber, C. R. Vidal, Discrete and continuous Franck Condon factors of the  $Mg_2 A^1\Sigma_u^+ - X^1\Sigma_g^+$  system and their  $J$  dependence, *J. Chem. Phys.* 66 (8) (1977) 3694–3704. doi:10.1063/1.434406.
- [20] W. J. Balfour, A. E. Douglas, Absorption spectrum of the  $Mg_2$  molecule, *Can. J. Phys.* 48 (7) (1970) 901–914. doi:10.1139/p70-116.
- [21] L. B. Knight, M. A. Ebener, Matrix isolation of  $Mg_2$  and  $Mg_n$  molecules in neon, argon, and nitrogen hosts, *J. Mol. Spectr.* 61 (3) (1976) 412–422. doi:10.1016/0022-2852(76)90332-5.
- [22] H. Lauterwald, K. Rademann, Direct absorption studies of jet-cooled metal dimers: Magnesium and cesium, *Ber. Bunsenges. Phys. Chem.* 96 (9) (1992) 1273–1275. doi:10.1002/bbpc.19920960940.
- [23] I. O. Antonov, B. J. Barker, V. E. Bondybey, M. C. Heaven, Spectroscopic characterization of  $Be_2^+ X^2\Sigma_u^+$  and the ionization energy of  $Be_2$ , *J. Chem. Phys.* 133 (7) (2010) 074309. doi:10.1063/1.3472977.
- [24] P. Dugourd, J. Chevalyere, C. Bordas, M. Broyer, Strontium clusters and ionization of the  $Sr_2$  dimer, *Chem. Phys. Lett.* 193 (6) (1992) 539–545. doi:10.1016/0009-2614(92)85845-2.
- [25] L. N. Ding, P. D. Kleiber, M. A. Young, W. C. Stwalley, A. M. Lyyra, Photodissociation spectroscopy of  $Mg_2^+$  ( $1^2\Sigma_u^+ - 1^2\Sigma_g^+$ ), *Phys. Rev. A* 48 (3) (1993) 2024–2030. doi:10.1103/PhysRevA.48.2024.
- [26] M. Sodupe, C. W. Bauschlicher, H. Partridge, A theoretical study of  $Mg(CO_2)_n^+$  and  $Sr(CO_2)_n^+$  for  $n = 1$  and 2 and  $Mg_2CO_2^+$ , *Chem. Phys. Lett.* 192 (2-3) (1992) 185–194. doi:10.1016/0009-2614(92)85450-0.
- [27] A. Ricca, C. W. Bauschlicher, The low-lying electronic states of  $Mg_2^+$ , *Chem. Phys. Lett.* 226 (5) (1994) 459–462. doi:10.1016/0009-2614(94)00756-X.
- [28] H. Ladjimi, D. Sardar, M. Farjallah, N. Alharzali, S. Naskar, R. Mlika, H. Berriche, B. Deb, Spectroscopic properties of the molecular ions  $BeX^+$  ( $X=Na, K, Rb$ ): Forming cold molecular ions from an ion–atom mixture by stimulated Raman adiabatic process, *Mol. Phys.* 116 (14) (2018) 1812–1826. doi:10.1080/00268976.2018.1458999.
- [29] N. Alharzali, D. Sardar, R. Mlika, B. Deb, H. Berriche, Spectroscopic properties and cold elastic collisions of alkaline-earth Mg +  $Mg^+$  system, *J. Phys. B: At. Mol. Opt. Phys.* 51 (19) (2018) 195201. doi:10.1088/1361-6455/aad6cb.
- [30] M. Śmiakowski, M. Tomza, Interactions and chemical reactions in ionic alkali-metal and alkaline-earth-metal diatomic  $AB^+$  and triatomic  $A_2B^+$  systems, *Phys. Rev. A* 101 (1) (2020) 012501. doi:10.1103/PhysRevA.101.012501.
- [31] M. Śmiakowski, T. Korona, M. Tomza, *Ab Initio* electronic structure of the  $Sr_2^+$  molecular ion, *J. Phys. B: At. Mol. Opt. Phys.* 53 (13) (2020) 135303. doi:10.1088/1361-6455/ab84c53w.
- [32] W. W. Smith, O. P. Makarov, J. Lin, Cold ion–neutral collisions in a hybrid trap, *J. Mod. Opt.* 52 (16) (2005) 2253–2260. doi:10.1080/09500340500275850.
- [33] L. Ratschbacher, C. Zipkes, C. Sias, M. Köhl, Controlling chemical reactions of a single particle, *Nat. Phys.* 8 (9) (2012) 649–652. doi:10.1038/nphys2373.
- [34] P. Eberle, A. D. Dörfler, C. von Planta, K. Ravi, S. Willitsch, A dynamic ion–atom hybrid trap for high-resolution cold-collision studies, *ChemPhysChem* 17 (22) (2016) 3769–3775. doi:10.1002/cphc.201600643.
- [35] M. Tomza, K. Jachymski, R. Gerritsma, A. Negretti, T. Calarco, Z. Idziaszek, P. S. Julienne, Cold hybrid ion-atom systems, *Rev. Mod. Phys.* 91 (3) (2019) 035001. doi:10.1103/RevModPhys.91.035001.
- [36] H. Hogreve,  $Mg_2^{2+}$ : A long-lived metastable dication, *Chem. Phys. Lett.* 394 (1) (2004) 32–36. doi:10.1016/j.cpllett.2004.06.099.
- [37] M. Génévriez, D. Wehrli, F. Merkt, High-resolution spectroscopy of the transition of  $MgAr^+$  by isolated-core multiphoton Rydberg dissociation, *Mol. Phys.* 118 (11) (2020) e1703051. doi:10.1080/00268976.2019.1703051.
- [38] D. Wehrli, M. Génévriez, S. Knecht, M. Reiher, F. Merkt, Complete characterization of the  $3p$  Rydberg complex of a molecular ion:  $MgAr^+$ . I. Observation of the  $Mg(3p\sigma)Ar^+ B^+$  state and determination of its structure and dynamics, *J. Chem. Phys.* 153 (7) (2020) 074310. doi:10.1063/5.0015603.
- [39] M. Génévriez, D. Wehrli, F. Merkt, Complete characterization of the  $3p$  Rydberg complex of a molecular ion:  $MgAr^+$ . II. Global analysis of the  $A^+ ^2\Pi$  and  $B^+ ^2\Sigma^+$  ( $3p\sigma, \pi$ ) states, *J. Chem. Phys.* 153 (7) (2020) 074311. doi:10.1063/5.0015608.
- [40] D. Wehrli, M. Génévriez, S. Knecht, M. Reiher, F. Merkt, Charge-transfer-induced predissociation in Rydberg states of molecular cations:  $MgAr^+$ , *J. Phys. Chem. A* 125 (31) (2021) 6681–6696. doi:10.1021/acs.jpca.1c03859.

- [41] M. Génévriez, D. Wehrli, T. Berglitsch, F. Merkt, Characterization of the  $3d\delta$  Rydberg state of  $\text{MgAr}^+$  using a quantum-control optical scheme, *Phys. Rev. A* 104 (4) (2021) 042811. doi:10.1103/PhysRevA.104.042811.
- [42] D. Wehrli, M. Génévriez, F. Merkt, Spectroscopic characterization of a thermodynamically stable doubly charged diatomic molecule:  $\text{MgAr}^{2+}$ , *Phys. Chem. Chem. Phys.* 23 (18) (2021) 10978–10987. doi:10.1039/D1CP00730K.
- [43] G. Reiser, W. Habenicht, K. Müller-Dethlefs, E. W. Schlag, The ionization energy of nitric oxide, *Chem. Phys. Lett.* 152 (2) (1988) 119–123. doi:10.1016/0009-2614(88)87340-8.
- [44] K. Müller-Dethlefs, E. W. Schlag, High-resolution zero kinetic energy (ZEKE) photoelectron spectroscopy of molecular systems, *Annu. Rev. Phys. Chem.* 42 (1991) 109–136.
- [45] W. A. Chupka, Factors affecting lifetimes and resolution of Rydberg states observed in zero-electron-kinetic-energy spectroscopy, *J. Chem. Phys.* 98 (6) (1993) 4520–4530. doi:10.1063/1.465011.
- [46] F. Merkt, S. Willitsch, U. Hollenstein, High-resolution photoelectron spectroscopy, in: *Handbook of high-resolution spectroscopy*, John Wiley & Sons, Ltd., 2011. doi:10.1002/9780470749593.hrs071.
- [47] M. Génévriez, D. Wehrli, J. Agner, F. Merkt, PFI-ZEKE photoelectron spectroscopy of positively charged ions: Illustration with  $\text{Mg}^+$ , *Int. J. Mass Spectrom.* 435 (2019) 209–216. doi:10.1016/j.ijms.2018.10.017.
- [48] D. Wehrli, M. Génévriez, C. Kreis, J. A. Agner, F. Merkt, Determination of the interaction potential and rovibrational structure of the ground electronic state of  $\text{MgAr}^+$  using PFI-ZEKE photoelectron spectroscopy, *J. Phys. Chem. A* 124 (2) (2020) 379–385. doi:10.1021/acs.jpca.9b10435.
- [49] M. A. Duncan, Laser vaporization cluster sources, *Rev. Sci. Instrum.* 83 (4) (2012). doi:10.1063/1.3697599.
- [50] S. Amaran, R. Kosloff, M. Tomza, W. Skomorowski, F. Pawlowski, R. Moszynski, L. Rybak, L. Levin, Z. Amitay, J. M. Berglund, D. M. Reich, C. P. Koch, Femtosecond two-photon photoassociation of hot magnesium atoms: A quantum dynamical study using thermal random phase wavefunctions, *J. Chem. Phys.* 139 (16) (2013) 164124. doi:10.1063/1.4826350.
- [51] K. J. R. Rosman, P. D. P. Taylor, Isotopic compositions of the elements 1997 (Technical Report), *Pure Appl. Chem.* 70 (1) (1998) 217–235. doi:10.1351/pac199870010217.
- [52] K. Müller-Dethlefs, E. W. Schlag, Chemical applications of zero kinetic energy (ZEKE) photoelectron spectroscopy, *Angew. Chem. Int. Ed.* 37 (10) (1998) 1346–1374. doi:10.1002/(SICI)1521-3773(19980605)37:10<1346::AID-ANIE1346>3.0.CO;2-H.
- [53] U. Hollenstein, R. Seiler, H. Schmutz, M. Andrist, F. Merkt, Selective field ionization of high Rydberg states: Application to zero-kinetic-energy photoelectron spectroscopy, *J. Chem. Phys.* 115 (12) (2001) 5461–5469. doi:10.1063/1.1396856.
- [54] D. Wehrli, U. Hollenstein, F. Merkt, Line shapes and line positions in PFI-ZEKE photoelectron and MATI spectra of positively charged ions, *Mol. Phys.* 119 (10) (2021) e1900613. doi:10.1080/00268976.2021.1900613.
- [55] A. Kramida, Y. Ralchenko, J. Reader, NIST Atomic Spectra Database (version 5.8) (2020). doi:10.18434/T4W30F.
- [56] R. N. Zare, *Angular Momentum: Understanding spatial aspects in chemistry and physics*, Wiley, New York, 1988.
- [57] R. R. Bennett, J. G. McCaffrey, W. H. Breckenridge, A spectroscopic characterization of the  $a\ ^3\Pi_{0-}$ ,  $a\ ^3\Pi_{0+}$ , and  $E\ ^3\Sigma^+$  states of the  $\text{MgAr}$  van der Waals molecule, *J. Chem. Phys.* 92 (5) (1990) 2740–2747. doi:10.1063/1.457919.
- [58] E. Czuchaj, M. Krośnicki, H. Stoll, Ab initio calculations for the potential curves and spin-orbit coupling of  $\text{Mg}_2$ , *Theor. Chem. Acc.* 107 (1) (2001) 27–32. doi:10.1007/s002140100296.
- [59] J. M. Merritt, A. L. Kaledin, V. E. Bondybey, M. C. Heaven, The ionization energy of  $\text{Be}_2$ , and spectroscopic characterization of the  $(1)\ ^3\Sigma_u^+$ ,  $(2)\ ^3\Pi_g$ , and  $(3)\ ^3\Pi_g$  states, *Phys. Chem. Chem. Phys.* 10 (27) (2008) 4006–4013. doi:10.1039/b803975e.
- [60] J. Xie, R. N. Zare, Selection rules for the photoionization of diatomic molecules, *J. Chem. Phys.* 93 (5) (1990) 3033–3038. doi:10.1063/1.458837.
- [61] J. K. G. Watson, Comment on “Selection rules for the photoionization of diatomic molecules” [*J. Chem. Phys.* 93, 3033 (1990)], *J. Chem. Phys.* 108 (2) (1998) 820–820. doi:10.1063/1.475445.
- [62] R. Signorell, F. Merkt, General symmetry selection rules for the photoionization of polyatomic molecules, *Mol. Phys.* 92 (5) (1997) 793–804. doi:10.1080/002689797169745.
- [63] G. Herzberg, *Molecular spectra and molecular structure*, Volume I, *Spectra of diatomic molecules*, 2nd Edition, Van Nostrand Reinhold Company, New York, 1950.
- [64] A. D. Buckingham, B. J. Orr, J. M. Sichel, *Angular distribution and intensity in molecular photoelectron spectroscopy I. General theory for diatomic molecules*, *Phil. Trans. Roy. Soc. Lond. A* 268 (1970) 147–157. URL <http://www.jstor.org/stable/73975>
- [65] F. Merkt, T. P. Softley, Rotational line intensities in zero kinetic energy photoelectron spectroscopy (ZEKE-PES), *Int. Rev. Phys. Chem.* 12 (2) (1993) 205–239. doi:10.1080/01442359309353282.
- [66] M. Tomza, Private communication (2021).